A Hybrid Density Functional Theory/Molecular Mechanics Study of Nickel−Iron Hydrogenase: Investigation of the Active Site Redox States

Patricia Amara,[†] Anne Volbeda,[†] Juan Carlos Fontecilla-Camps,*[,‡] and Martin J. Field*[,†]

Contribution from the Laboratoire de Dynamique Moléculaire and Laboratoire de Cristallographie et Cristallogenèse des Protéines Institut de Biologie Structurale—Jean-Pierre Ebel, CEA/CNRS 41, rue Jules Horowitz, F-38027 Grenoble Cedex 01, France

Received November 17, 1998. Revised Manuscript Received March 9, 1999

Abstract: We have investigated using theoretical methods some of the redox states of the active site of *Desulfovibrio gigas* NiFe hydrogenase, which is a metalloprotein that catalyzes the reversible reaction $H_2 \rightleftharpoons 2H^+ + 2\ e^-$. A hybrid potential that combines *ab initio* density functional theory and a molecular mechanics energy function was employed. Starting from the X-ray structure of the oxidized form refined at 2.54 Å resolution, we have optimized the structures of the active site redox states, believed to be involved in the activation and the catalytic cycle of the enzyme, and compared them with the available X-ray data. We have also tested various hypotheses concerning the oxidation states of the Ni−Fe bimetallic center and the protonation states of the active site by comparing calculated spin densities and vibrational frequencies with EPR and IR spectroscopic data. The good agreement we have obtained with experiment allows us to identify more precisely those structures that are likely to be important in the enzymatic reaction mechanism.

1. Introduction

Numerical methods, such as molecular dynamics and Monte Carlo simulation techniques, are increasingly important tools for studying the structure and function of biomacromolecules.[1−3] Owing to the complexity and the size of macromolecular systems, it is common practice to use empirical potentials or molecular mechanics (MM) force fields to calculate the system's energy and the forces on its atoms.[4] With these approximate functions, it is possible to study systems comprising thousands of atoms. Modeling chemical reactions in which bonds are broken and formed is, however, not straightforward using empirical potentials because of the difficulties of choosing an analytic form for the energy surface and parametrizing it. In contrast, quantum mechanical (QM) methods do, in principle, allow an accurate description of reactive processes because they can determine changes in a molecule's electron density as its geometry changes. The problem with these methods, though, is that they are expensive, and so it is impractical to treat macromolecular systems routinely even though there have been significant recent algorithmic advances and computers are continually improving in speed.[5] A solution to this dilemma has been to develop hybrid QM/MM potentials in which a system is partitioned into two or more regions.[6−8] For the simplest case of two regions, there will be a small region in which the reaction occurs and whose atoms are treated with a QM potential, and a larger region, comprising the remainder of the atoms, which is treated with a simpler MM potential. For reviews on the wide variety of hybrid potentials that have been developed see, for example, refs 9 and 10.

In this work, we have employed a hybrid QM/MM potential method for the investigation of some of the redox states of the hydrogenase from the sulfate-reducing bacterium *Desulfovibrio (D.) gigas*, which catalyzes the reversible reaction $H_2 \rightleftharpoons 2H^+ + 2e^-$ under anaerobic conditions. Until a few years ago, it was believed that the active site of the enzyme consisted of a nickel atom with either pure S or S, (N,O) mixed coordination.[11] In 1995, however, with the solution of the first X-ray structure of hydrogenase from *D. gigas* (an oxidized form at 2.85 Å resolution), it became evident that the active site, which appeared to be deeply buried in the enzyme at approximately 30 Å from the protein surface, was not mononuclear; rather, there was another unidentified transition metal close to the nickel.[12] The identity of the second metal was proven to be iron using X-ray data collected to 3.00 Å resolution on both sides of the Fe absorption edge,[13] and this was later confirmed by ENDOR using ^{57}Fe.[14] Another crystallographic analysis, this time at 2.54 Å resolution, revealed a second unusual characteristic of the active site, namely the presence of three nonproteic, diatomic

[†] Laboratoire de Dynamique Moléculaire.

[‡] Laboratoire de Cristallographie et Cristallogenèse des Protéines.

(1) Allen, M. P.; Tildesley, D. J. *Computer Simulations of Liquids*; Oxford University Press: Oxford, 1987.

(2) McCammon, J. A.; Harvey, S. *Dynamics of Proteins and Nucleic Acids*; Cambridge University press: Cambridge, 1987.

(3) Brooks, C. L., III; Karplus, M.; Pettitt, B. M. *Adv. Chem. Phys.* **1988**, *71*, 1.

(4) Burkett, U.; Allinger, N. L. *Molecular Mechanics*; American Chemical Society: Washington, DC, 1982.

(5) Friesner, R. A.; Beachy, M. D. *Curr. Opin. Struct. Biol.* **1998**, *8*, 257−62.

(6) Warshel, A.; Levitt, M. *J. Mol. Biol.* **1976**, *103*, 227−49.

(7) Singh, U. C.; Kollman, P. A. *J. Comp. Chem.* **1986**, *7*, 718−30.

(8) Field, M. J.; Bash, P. A.; Karplus, M. *J. Comp. Chem.* **1990**, *11*, 700−33.

(9) Gao, J. In *Reviews in Computational Chemistry: Methods and Applications of Combined Quantum Mechanical and Molecular Mechanical Potentials*; Lipkowitz, K. B., Boyd, D. B., Eds; VCH Publishers: New York, 1996.

(10) Amara, P.; Field, M. J. In *The Encyclopedia of Computational Chemistry;* Schleyer, P. v. R., Schaefer, H. F., III, Schreiner, P. R., Eds; John Wiley & Sons: Chichester, 1998; pp 1−7.

(11) Albracht, S. P. J. *Biochim. Biophys. Acta.* **1994**, *1188*, 167−204.

(12) Volbeda, A.; Charon, M. H.; Piras, C.; Hatchikian, E. C.; Frey, M.; Fontecilla-Camps, J. C. *Nature* **1995**, *373*, 580−7. Cammack, R. *Nature* **1995**, *373*, 556−7.

10.1021/ja983971b CCC: $18.00
Published on Web 04/20/1999

ligands bound to the iron.[13] It was inferred that these ligands were probably responsible for the three, exceptionally-high-frequency, infrared (IR) bands that were earlier reported for the NiFe hydrogenase of *Chromatium vinosum*[15] and then for the *D. gigas* enzyme.[13,16] Later, Happe *et al.* identified the ligands as two CN^- and one CO after studying the shifts in the IR bands in enriched ^{13}C and ^{15}N samples.[17] These ligands are believed to stabilize both low redox and low spin states of the iron. Despite the recent controversy about the identity of these ligands raised by the resolution of a NiFe hydrogenase structure from *D. vulgaris Miyazaki*,[18] we believe that there is sufficient experimental evidence for the presence of two CN^- and one CO in *D. gigas* and in very similar hydrogenases from *D. fructosovorans*[19] and *Desulfomicrobium baculatum*[20] to warrant their inclusion in the model of the active site that we have adopted for our simulations.

In addition to the metals at the active site, the enzyme contains one [3Fe−4S] cluster and two [4Fe−4S] clusters that are likely to be involved in the transfer of the electrons resulting from the redox reaction at the active site because they are reduced during hydrogen uptake.[21] In this work, we have not studied the redox changes of these clusters and have focused on the active center instead. The center of the proximal cluster is located approximately 13 Å away from the nickel atom, and there is some debate about whether it could be directly involved in the catalytic mechanism.[21,22] We have not addressed this issue here as it would have been computationally intractable for us to treat so many atoms quantum mechanically in our calculations. The structural model also includes a NiFe bridging ligand, possibly an oxo anion which has been proposed to disappear upon reductive activation of the enzyme.[13,20] The active site of the 2.54 Å resolution structure is shown in Figure 1a.

Although numerous experiments have been and are being conducted to elucidate the mechanism of the enzyme, no unique picture has yet emerged. EPR experiments[11,23,24] showed that the enzyme can exist in many different redox states. This was later confirmed by IR experiments on the nonproteic ligands of the iron. Two oxidized forms of the enzyme give rise to two distinct nickel EPR signals called Ni−A and Ni−B.[25] Ni−A corresponds to an unready inactive form of the enzyme that needs a long reductive activation. Ni−B, the so-called ready form, is activated within seconds.[26] The crystals used for the initial *D. gigas* X-ray structure determination contained mainly Ni−A.[12] Under hydrogen pressure, the EPR signal of Ni−A ($S = {}^1/_2$) disappears and a new EPR signal called Ni−C ($S = {}^1/_2$) is detected after a transition, involving several EPR silent forms, Ni−SU, Ni−SI1, and Ni−SI2 as revealed by IR titrations of the different redox states of *D. gigas*.[13,16] Further reduction leads to the most reduced stable form of hydrogenase, called Ni−R, which is also EPR silent. When the active site was supposed to be mononuclear, several mechanisms were proposed, namely, (a) the Ni went from Ni(III) to Ni(0),[11] (b) only Ni(II) and Ni-(III) were involved,[21,27] and (c) the sulfurs from the cysteines of the active site could form radicals.[28,29] However, some of these proposals are difficult to reconcile with XAS experiments that seem to indicate that the Ni center does not undergo major electron density changes through the catalytic cycle as there are no significant shifts of the Ni absorption edge except for the Ni−A → Ni−SI transition.[30] In addition, such mechanisms could not consider a redox role for the Fe as it was not known to exist at the time. Redox changes at the Fe atom have been suggested to be responsible for the shifts of the high-frequency IR bands that are observed for different enzyme intermediates.[13,16] However, these shifts could also be due to changes in the environment of the Fe atom. There are also other questions that remain to be clarified concerning, for example, the nature of the active site hydrogen species involved in the mechanism, because the catalysis proceeds through a heterolytic cleavage of H_2[31] and so the active site must contain binding sites for hydrides and protons. Two putative binding sites have been proposed[13] that correspond to two coordination sites of the Ni, one of which is axial and the other of which is shared with the Fe (see Figure 1a). It is also possible that the thiolate ligands act as bases. Because of these uncertainties, many mechanisms are conceivable which differ in the number of bound hydrides in the different stable reaction intermediates and in the charges and spin states of the metal centers and their ligands.

The first theoretical attempt to model the mechanism of hydrogenase was performed by Pavlov *et al.*[32] They used density functional theory (DFT) calculations with the B3LYP functional[33,34] to study a model of the active site in vacuum and proposed a mechanism for the molecular hydrogen uptake. However, as the structural environment was not taken into account, their mechanism exhibited rather large movements of the ligands (i.e., a cyanide ligand going from a terminal to a position bridging the bimetallic center) which would seem to

(13) Volbeda, A.; Garcin, E.; Piras, C.; De Lacey, A. L.; Fernandez, V. M.; Hatchikian, E. C.; Frey, M.; Fontecilla-Camps, J. C. *J. Am. Chem. Soc.* **1996**, *118*, 12989−96.

(14) Huyett, J. E.; Carepo, M.; Pamplona, A.; Moura, I.; Moura, J. J. G.; Hoffman, B. M. *J. Am. Chem. Soc.* **1997**, *119*, 9291−92.

(15) Bagley, K. A.; Duin, E. C.; Roseboom, W.; Albracht, S. P. J.; Woodruff, W. H. *Biochemistry* **1995**, *34*, 5527−35.

(16) De Lacey, A. L.; Hatchikian, E. C.; Volbeda, A.; Frey, M.; Fontecilla-Camps, J. C.; Fernandez, V. M. *J. Am. Chem. Soc.* **1997**, *119*, 7181−89.

(17) Happe, R. P.; Roseboom, W.; Pierik, A. J.; Albracht, S. P. J.; Bagley, K. A. *Nature* **1997**, *385*, 126.

(18) Higuchi, Y.; Yagi, T.; Yasuoka, N. *Structure* **1997**, *5*, 1671−80.

(19) Montet Berthéas, Y. Elucidation des Mécanismes d'action des hydrogénases à Ni−Fe: Etude de l'hydrogénase de Desulfovibrio fructosovorans et de ses mutants par cristallographie des rayons X. Thèse de l'Université Joseph Fourier, Grenoble, France, 1998.

(20) Garcin, E.; Vernede, X.; Hatchikian, E. C.; Volbeda, A.; Frey, M.; Fontecilla-Camps, J. C. *Structure*. In press.

(21) Teixeira, M.; Moura, I.; Xavier, A. V.; Moura, J. G.; LeGall, J.; DerVartanian, D. V.; Peck, H. D., Jr.; Huynh, B. H. *J. Biol. Chem.* **1989**, *264*, 16435−50.

(22) Coremans, J. M. C. C.; Van Garderen, C. J.; Albracht, S. P. J. *Biochim. Biophys. Acta* **1992**, *1119*, 148−56.

(23) Moura, J. J. G.; Moura, I.; Huynh, B. H.; Krüiger, H. J.; Teixeira, M.; Du Varney, R. G.; Der Vartanian, D. G.; Ljungdahl, P.; Xavier, A. V.; Peck, H. D., Jr.; LeGall, J. *J. Biochem. Biophys. Res. Commun.* **1982**, *108*, 1388−93.

(24) Cammack, R.; Patil, O. S.; Hatchikian, E. C.; Fernandez, V. M. *Biochim. Biophys. Acta* **1987**, *912*, 98−109.

(25) The formalism that labels the different redox states as Ni−A, Ni−SI, Ni−C, Ni−R etc. will be employed here. This notation was initially used in EPR studies and later adopted in IR studies as well.

(26) Fernandez, V. M.; Hatchikian, E. C.; Cammack, R. C. *Biochim. Biophys. Acta* **1985**, *832*, 69−79.

(27) Hatchikian, E. C.; Fernandez, V. M.; Cammack, R. In *Microbiology and Biochemistry of strict anaerobes involved in interspecies hydrogen transfer. FEMS Symposium*; Belaich, J. P., Bruschi, H., Garcia, J. L., Eds.; Plenum Press: New York, 1990.

(28) Dole, F.; Fournel, A.; Magro, V.; Hatchikian, E. C.; Bertrand, P.; Guigliarelli, B. *Biochemistry* **1997**, *36*, 7847−54.

(29) Maroney, M. J. In *Encyclopedia of Inorganic Chemistry*; King, R. B., Ed.; Wiley & Sons: Chichester, 1994.

(30) Gu, Z.; Dong, J.; Allan, C. B.; Choudhury, S. B.; Franco, R.; Moura, J. J. G.; Moura, I.; LeGall, J.; Przybyla, A. E.; Roseboom, W.; Albracht, S. P. J.; Axley, M. J.; Scott, R. A.; Maroney, M. J. *J. Am. Chem. Soc.* **1996**, *118*, 11155−65.

(31) Krasna, A. L.; Rittenberg, D. *J. Am. Chem. Soc.* **1954**, *76*, 3015.

(32) Pavlov, M.; Siegbahn, P. E. M.; Blomberg, R. A.; Crabtree, R. H. *J. Am. Chem. Soc.* **1998**, *120*, 548−55.

(33) Parr, R. G.; Yang, W. *Density-Functional Theory of Atoms and Molecules*; Clarendon Press: Oxford, 1989.

(34) (a) Becke, A. D. *Phys. Rev.* **1988**, *A38*, 3098. (b) Becke, A. D. *J. Chem. Phys.* **1993**, *98*, 1372−77. (c) Becke, A. D. *J. Chem. Phys.* **1993**, *98*, 5648.

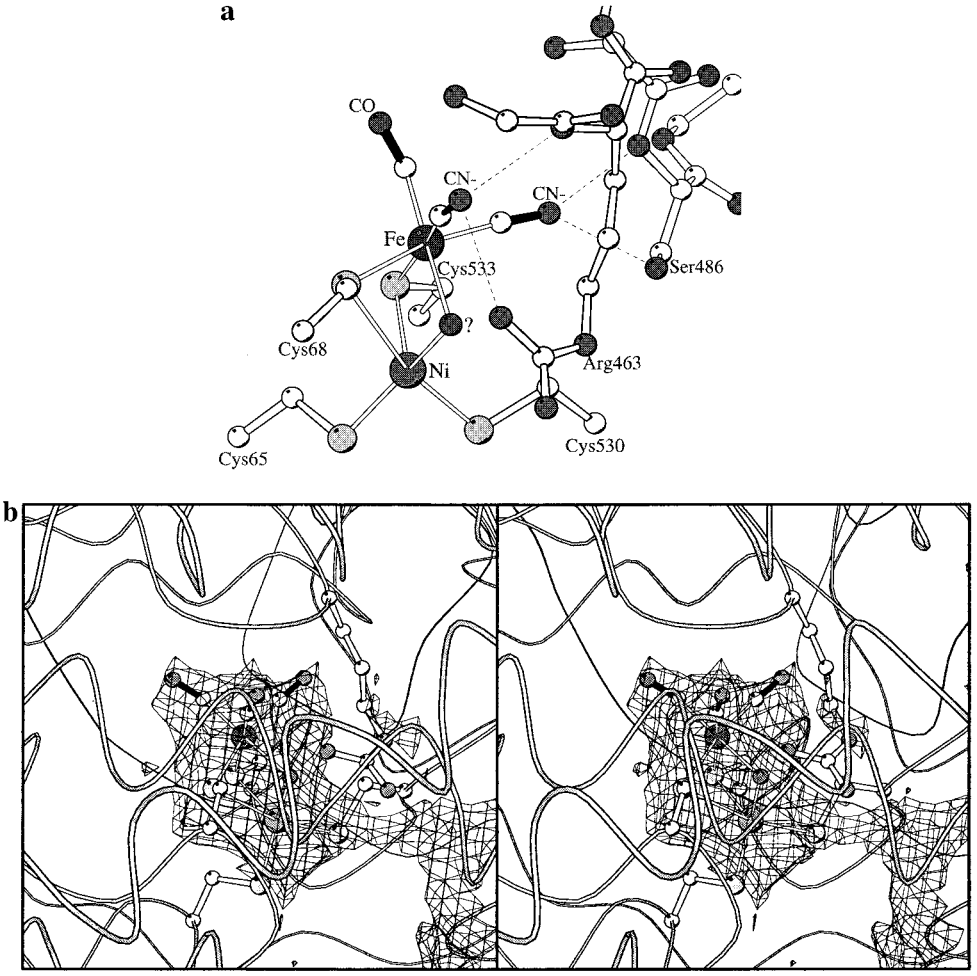

Figure 1. (a) Active site of *D. gigas* hydrogenase; dashed lines are the possible hydrogen bonds of the cyanides, which are ligands of the Fe atom, to the protein. The figure is based upon the X-ray structural data of the oxidized, inactive form of the enzyme. The question mark indicates the presence of a bridging ligand which has been putatively assigned to an oxo anion. There is a vacant binding site of the Ni atom trans to Cys 533. (b) Stereographic view of the hydrogenase active site cavity map calculated with a probe radius of 1 Å, after omitting all the active site atoms, i.e., the Ni, Fe, and their ligands, from the refined model. The main chain atoms of the cysteine ligands were not omitted and the protein main chain is shown as a ribbon. The calculation shows that the active site is connected via the nickel to a H_2 gas accessible channel going to the surface[47] and the diatomic iron ligands are completely buried in the protein environment with little freedom for movement.

be precluded in the enzyme. Figure 1b shows that such a transfer would require major conformational changes of the active site environment, i.e. the rest of the enzyme. We will show here that the inclusion of the environment of the active site seems to be crucial for a good representation of the system. In our work, we have applied a hybrid DFT/MM algorithm to the simulation of several redox states of hydrogenase to investigate the structural and electronic changes that occur in the catalytic cycle of the enzyme. The problem we have addressed is the role of the different atoms at the active site, i.e., which atoms among the Fe, Ni, and the sulfur atoms are involved in the catalytic redox chemistry of hydrogenase. Because of the size and complexity of the hydrogenase system, these calculations represent an especially challenging application of the hybrid potential approach.

The outline of this paper is as follows. Section 2 describes the theoretical techniques that we have used to study the system, section 3 discusses the results we obtained, and section 4 gives the conclusions.

2. Modeling and Simulating the Enzyme

2.1. The Hybrid Potential. The description of the electronic structure of atoms rich in electrons and, in particular, transition metals is a demanding task for quantum chemical methods. Although it is possible to use high-level *ab initio* molecular orbital methods to study such systems,[35] it has become increasingly apparent that *ab initio* methods based upon density functional theory offer an alternative that is often as precise and yet more efficient.[33,36,37] In contrast, empirical and semiempirical QM methods for studying transition metals are much less well developed. In our hybrid potential we have chosen to combine a DFT Kohn−Sham (KS) method with a MM potential. We follow the same basic procedure as that used by one of us (M.J.F.) in the development of a semiempirical QM/MM hybrid potential.[8]

We divide the system up into two regions, a QM region and a MM region (see Figure 2). The total energy, E, will be a functional of the electron density, ρ, in the QM region and can be written as

$$E[\rho] = E_{QM}[\rho] + E_{MM} + E_{QM/MM}[\rho] \quad (2.1)$$

The first term on the right-hand side of this equation, E_{QM}, is the usual DFT energy expression[33] and is

$$E_{QM}[\rho] = T_s[\rho] + J[\rho] + E_{xc}[\rho] + \int d\mathbf{r}\, \rho(\mathbf{r}) V_{QM}(\mathbf{r}) \quad (2.2)$$

where T_s, J, and E_{xc} are the kinetic, Coulomb, and exchange-correlation

(35) Hehre, W. J.; Radom, L.; Schleyer, P. v. R.; Pople, J. A. *Ab Initio Molecular Orbital Theory*; J. Wiley & Sons: New York, 1986.
(36) Salahub, D. *Adv. Chem. Phys.* **1987**, *69*, 447.
(37) Stephens, P. J.; Devlin, F. J.; Chabalowski, C. F.; Frisch, M. J. *J. Phys. Chem.* **1994**, *98*, 11623−27.

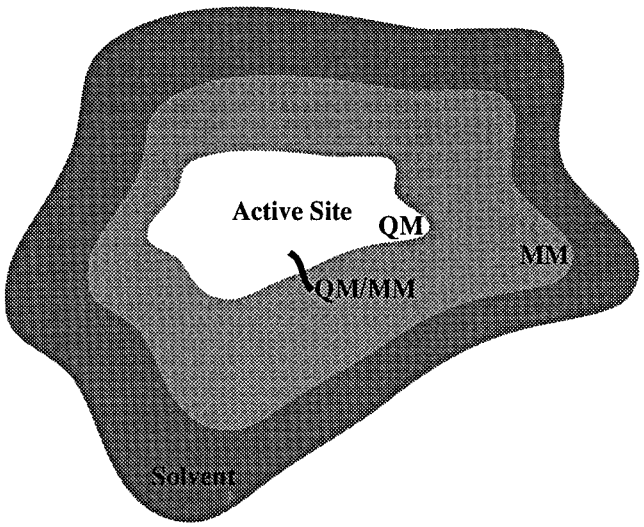

Figure 2. A schematic diagram of the partitioning of a system in the QM/MM formalism.

energies, respectively. The last term on the right-hand side is the interaction energy between the electron density and the potential due to the nuclei of the QM atoms, V_{QM}. **r** is a position vector.

The second term of eq 2.1, E_{MM}, is the energy of the atoms in the MM region and is independent of the electron density. For the type of force field that we are using, it is the sum of energies due to covalent interactions (the bonds, bond angles, proper and improper dihedral angles) and nonbonding interactions (Coulomb and Lennard-Jones), i.e.

$$E_{MM} = E_{bond} + E_{angle} + E_{dihedral} + E_{improper} + E_{Coulomb} + E_{Lennard-Jones} \quad (2.3)$$

The third term of eq 2.1, $E_{QM/MM}$, is the interaction energy between the QM and MM regions. It consists of three parts:

$$E_{QM/MM}[\rho] = E^{el}_{QM/MM}[\rho]\, E^{LJ}_{QM/MM} + E^{misc}_{QM/MM} \quad (2.4)$$

There will be an electrostatic energy, $E^{el}_{QM/MM}$, due to the interactions between the partial charges on the atoms in the MM region and the electrons and nuclei of the atoms in the QM region. This will have the form

$$E^{el}_{QM/MM} = \sum_{\alpha m} \frac{Z_\alpha Q_m}{r_{\alpha m}} + \int d\mathbf{r}\, \rho(\mathbf{r}) V_{QM/MM}(\mathbf{r}) \quad (2.5)$$

where Z is a nuclear charge, Q is a charge on an MM atom and $r_{\alpha m}$ is an interparticle distance. The subscripts α and m refer to nuclei and MM atoms, respectively. $V_{QM/MM}$ is the potential due to the charges on the MM atoms and takes the form

$$V_{QM/MM}(\mathbf{r}) = -\sum_m \frac{Q_m}{|\mathbf{r} - \mathbf{r}_m|} \quad (2.6)$$

The second and third components of the QM/MM interaction are independent of the electron density. The second term is a Lennard-Jones interaction between the QM and MM atoms that has the standard form

$$E^{LJ}_{QM/MM} = \sum_{\alpha m} \left\{ \frac{A_{\alpha m}}{r^{12}_{\alpha m}} - \frac{B_{\alpha m}}{r^{6}_{\alpha m}} \right\} \quad (2.7)$$

The third term of eq 2.4 comprises miscellaneous MM terms and arises in those cases, such as hydrogenase, where a single molecule is partitioned between the QM and MM regions. In these instances there will be covalent bonds between QM and MM atoms and it is necessary to devise methods in which the electron density along the bonds between the QM and MM atoms is terminated. Several such schemes have been proposed including methods based upon hybrid orbitals[38,39] and embedding techniques.[40] Here, we use the simple "link atom" method which has been shown to be reasonably effective.[7,8] In this technique, extra link atoms (usually hydrogens) are introduced along the QM/MM bonds at an appropriate distance (of the order of 1 Å) from the QM atom. Because extra unphysical atoms have been introduced into the system, the interactions between these atoms and the rest of the system have to be parametrized (as, incidentally, is the case with all the other methods). In this study, we use the following scheme that works well.[8] The link atoms are invisible to the MM atoms but are included in the QM calculation as normal. All the other QM atoms including those bound to the link atoms feel the full electrostatic potential due to the MM atoms.

The link atoms are QM atoms and are included only in the QM calculation. The extra MM terms (the third component of $E_{QM/MM}$) arise because there are MM bond, bond angle, and dihedral terms between QM and MM atoms at the boundaries of the QM and MM regions. The criterion for including these terms is that an MM term is retained whenever it involves at least one MM atom. Note that, whereas all the electrostatic interactions between QM and MM atoms are calculated even at the boundaries, the Lennard-Jones terms are treated in the normal way. That is, they are calculated only for atoms separated by three or more covalent bonds.

With the energy expression of eq 2.1 fully defined, the Kohn−Sham procedure can be applied to obtain the KS orbitals, the electron density, and, thus, the energy of the system. If the KS orbitals are denoted ϕ^α and ϕ^β for the electrons of α and β spin respectively, the electron density is

$$\rho(\mathbf{r}) = \sum_{i=1}^{N_\alpha} |\phi^\alpha_i(\mathbf{r})|^2 + \sum_{j=1}^{N_\beta} |\phi^\beta_j(\mathbf{r})|^2 \quad (2.8)$$

where N_α and N_β are the numbers of spin α and spin β electrons.

It is normal to expand the KS orbitals in terms of a basis set (in our case, Gaussians) and then variationally optimize the energy expression of eq 2.1 with respect to the basis set expansion coefficients. The one-electron equations that result and that need to be solved for the KS orbitals are little changed from the normal KS equations with the exception of the extra term, $V_{QM/MM}$, in the effective potential. Once the KS orbitals are known, the total energy of the system and the derivatives of the energy with respect to the atomic positions (both QM and MM) can be calculated in the normal way.

2.2. The Starting Model. The X-ray structure of hydrogenase determined at 2.54 Å resolution with structural waters included[13] was chosen as the starting model for our simulations. We first performed a pK_a calculation to assign the protonation states of all amino acid residues in the system using the program UHBD[41] and the "cluster method".[42] Our calculations gave an isoelectric point of 5.2 which compares well with the experimental value of 6.0.[43] Having determined the protonation states, the coordinates of all the hydrogens were determined using the option HBUILD[44] in version 23 of the molecular modeling program CHARMM[45] and the all-atom CHARMM force field.[46] To validate the molecular mechanics model we performed a 300 ps molecular dynamics simulation of the protein at a temperature of 300 K.[47] There is a good

(38) Théry, V.; Rinaldi, D.; Rivail, J.-L.; Maigret, B.; Ferenczy, G. G. *J. Comp. Chem.* **1994**, *15*, 269.
(39) Gao, J.; Amara, P.; Alhambra, C.; Field, M. J. *J. Phys. Chem. A* **1998**, *102*, 4714.
(40) Svensson, M.; Humbel, S.; Morokuma, K. *J. Chem. Phys.* **1996**, *100*, 19357−63.
(41) Davis, M. E.; Madura, J. D.; Luty, B. A.; McCammon, J. A. *Comp. Phys. Comm.* **1991**, *62*, 187.
(42) Antosiewicz, J.; McCammon, J. A.; Gilson, M. K. *J. Mol. Biol.* **1994**, *238*, 415.
(43) Cammack, R.; Fernandez, V.M.; Hatchikian, E.C. *Meth. Enzymol.* **1994**, *243*, 43−68.
(44) Brünger, A. T.; Karplus, M. *Proteins: Struct. Funct. Genet.* **1988**, *4*, 148−56.
(45) Brooks, B. R.; Bruccoleri, R. E.; Olafson, B. D.; States, D. J.; Swaminanathan, S.; Karplus, M. *J. Comp. Chem.* **1983**, *4*, 187−217.

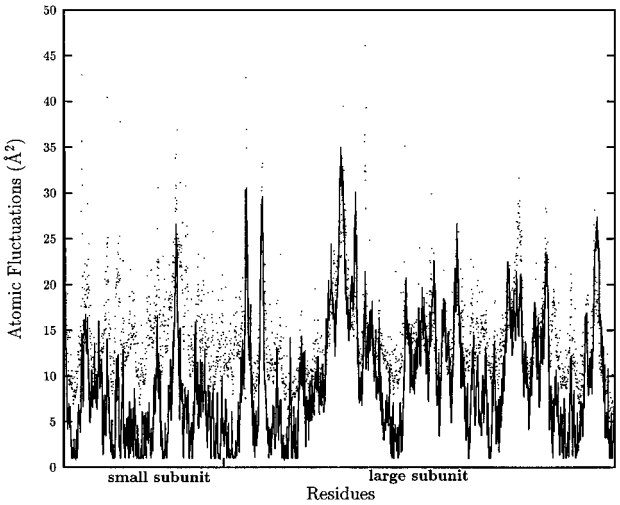

Figure 3. Atomic fluctuations for hydrogenase obtained from a 300 ps molecular dynamics simulation (dots) compared with the crystallographically refined temperature factors of the X-ray structure (line).

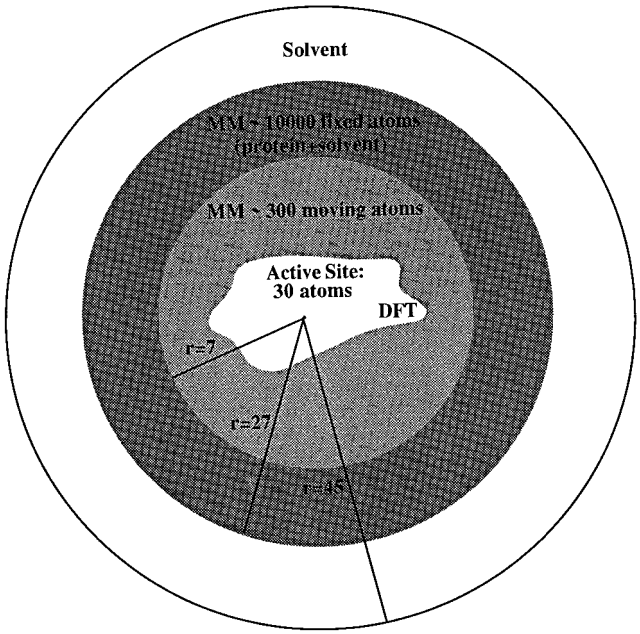

Figure 4. A schematic diagram of our modeled hydrogenase system (radii are given in Å). The solvent in the outer part is omitted after the initial molecular dynamics.

correlation between the fluctuations in the atomic positions arising during the simulation and the crystallographically refined temperature factors (see Figure 3).

For our calculations with the hybrid potential, we solvated the protein by placing it inside a sphere of water molecules of 45 Å radius and performing a 20 ps molecular dynamics simulation at a temperature of 300 K. This system was reduced from 36 000 to about 10 000 atoms by removing all atoms lying further away from the active site than 27 Å (see Figure 4). The removal was done in such a way that if an atom in a particular amino acid residue or water molecule was closer than

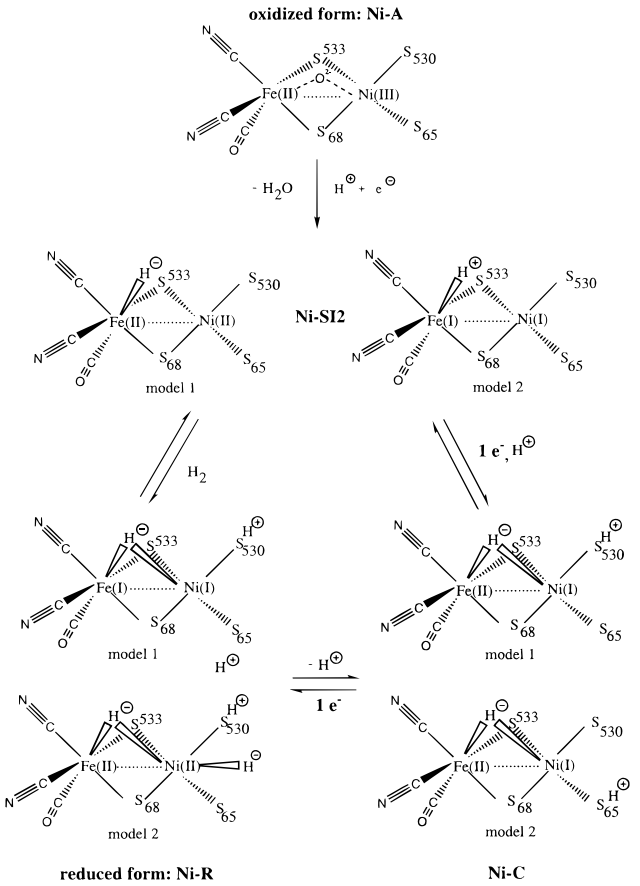

Figure 5. Starting models for the different states of the enzyme that were simulated.[13] Two models are proposed for the Ni−SI2, Ni−C, and Ni−R forms.

27 Å to the center of the active site the whole residue or molecule was kept. This ensured that the resulting model had an integer charge and that problems caused by "dipole-splitting" were minimized. The QM region consisted of about 30 atoms (depending upon the redox state) and was composed of, at least, the NiFe center, the 4 cysteine side chains bound to the nickel and iron atoms, and the 3 nonproteic diatomic ligands. Four hydrogen link atoms were introduced at the boundary of the QM and MM regions and were placed along each of the C_β(QM)−C_α(MM) bonds of the cysteines bound to the nickel. The remainder of the atoms were treated with the CHARMM all-atom MM force field. All electrostatic and Lennard-Jones interactions between the atoms of the QM and MM regions were calculated without truncation. In all our hybrid potential calculations on this system, atoms placed further than 7 Å from the iron atom were fixed. That is, they were not allowed to move although they did, of course, interact with the atoms within the 7 Å sphere. This gave about 300 free MM atoms in addition to 30 QM atoms.

2.3. The Proposed Mechanism. We have concentrated our calculations on a mechanism that has already been partially suggested and is mainly based upon data derived from X-ray crystallography and spectroscopic studies.[13,48] The choice of reaction intermediates was based on the idea of minimal conformational changes because the active center is deeply buried within the protein (see Figure 1b). Consequently, in our simulations we started from the X-ray structure of the oxidized form (the only one that was available at the beginning of this study) and introduced the changes on the active site required to mimic the redox transitions. The scheme of the catalytic cycle that we tested, together with the corresponding redox and coordination changes for both metals, is shown in Figure 5. From the most oxidized to the most reduced form, the redox states we have studied are as follows:

(46) Mackerell, A. D., Jr.; Bashford, D.; Bellott, M.; Dunbrack, R. L., Jr.; Evanseck, J. D.; Field, M. J.; Fischer, S.; Gao, J.; Guo, H.; Ha, S.; Joseph-McCarthy, D.; Kuchnir, L.; Kuczera, K.; Lau, F. T. K.; Mattos, C.; Michnick, S.; Ngo, T.; Nguyen, D. T.; Prodhom, B.; Reiher, W. E., III; Roux, B.; Schlenkrich, M.; Smith, J. C.; Stote, R.; Straub, J.E.; Watanabe, M.; Wiókiewicz-Kusczera, J.; Yin, D.; Karplus, M. *J. Phys. Chem. B* **1998**, *102*, 3586−616.

(47) Montet, Y.; Amara, P.; Volbeda, A.; Vernede, X.; Hatchikian, E. C.; Field, M. J.; Frey, M.; Fontecilla-Camps, J. C. *Nature Struct. Biol.* **1997**, *4*, 523−6.

(48) Montet, Y.; Garcin, E.; Volbeda, A.; Hatchikian, E. C.; Frey, M.; Fontecilla-Camps, J. C. *Pure Appl. Chem.* **1998**, *70*, 25−31.

Ni−A is the most oxidized form of hydrogenase that is obtained in, as-prepared, aerobic conditions and is inactive. EPR experiments of this state, in which the reduced form of hydrogenase was exposed to $^{17}O_2$, had suggested that there was an oxygenated species closely bound to the nickel.[49] In the 2.54 Å resolution X-ray structure of Ni−A, a bridging ligand between the two metals is found which, based on the shape of the electronic density, is probably monoatomic.[13] Following the crystallographic evidence, we have advanced the hypothesis that there is a bridging oxo group in this state. In the X-ray model, the oxo refined to an asymmetric position which is closer to the nickel than to the iron.[13] This unusual arrangement has been observed before by Churchill et al.,[50] although only for the higher row transition metals, tungsten and osmium.

Ni−SI (Ni−SI1 and Ni−SI2) has been found in IR experiments to be an intermediate in the transition from the Ni−A to the Ni−C state. Ni−SI2 is the form that may bind the H_2 molecule and lead to Ni−R. It also appears to arise from the protonation of Ni−SI1.[16]

Ni−C is one of the most studied forms experimentally and the only EPR active form in the catalytic cycle. It arises when the "as-prepared" enzyme is reduced under hydrogen. Two types of exchangeable hydrogen nuclei in the vicinity of the Ni atom have been revealed by ENDOR experiments.[51]

Ni−R is the most reduced form and results from the binding of a H^+ and a H^- (the reaction products) to Ni−SI2.

The main uncertainty we had in building some of the structures concerned those states in which there was a choice of protonation site at the active center (i.e., the cysteines as well as the empty binding sites of the Ni atom). It appeared unlikely that either Cys 68 or Cys 533 would act as such sites as they bridge the bimetallic center (see Figure 1a) and consequently split their electronic density between the two metals. This leaves Cys 65 and Cys 530 as possible candidates so we tried both in our calculations.

2.4. The Simulation Protocol. All hybrid potential calculations were performed using the quantum mechanical CADPAC program[52] that we modified by adding appropriate MM routines. For the DFT calculations we used a double-ζ quality basis set[53] for all non-metal atoms. For the transition metals, we employed effective core potentials to model the 1s, 2s, and 2p electrons (neon-like core) and the corresponding basis set for the valence electrons.[54] B3LYP/ECP DFT calculations have already been performed for other iron complexes and shown to give good results.[55] We employed the B3LYP exchange-correlation functional and used a relatively dense grid, of approximately 20 000 points per atom, for the integration of the exchange-correlation energy and potential terms.

For each redox state, the protons and bridging ligands were added to the active site when relevant (see section 3). The energy of the starting structure corresponding to a particular redox state was then calculated with the hybrid DFT/MM potential for different multiplicities and spin states. The spin states were typically very close in energy and when possible we have kept the one corresponding to the EPR experimental value of the spin. We will describe the problems we encountered in doing so in the next section. Once the DFT Kohn−Sham orbitals were obtained for a particular redox and spin state, the structure was optimized with the hybrid potential. Because these are CPU intensive calculations we adopted a fairly lax convergence criterion for the optimization process which was that the RMS gradient should fall below 0.5 kcal mol^{-1} Å^{-1}. Typically, 100 energy and derivative calculations were required per structure for the optimization to converge. After the optimization of the complete structure, the positions of the three nonproteic ligands bound to the iron were further optimized with all the remaining atoms fixed (RMS gradient below 0.2 kcal mol^{-1} Å^{-1}). The frequencies for these six atoms were then calculated by finite differences using the standard procedure for a normal mode analysis. It should be emphasized that the hybrid potential for the full 10 000 atom system was used in the last two steps even though all but six atoms were fixed. As a check of this reduced normal mode calculation, a normal mode calculation was performed for one structure for all the QM atoms. The relevant frequencies proved to be very similar (to within 0.5 cm^{-1}) to the ones obtained with all but the three diatomic ligands fixed.

In addition to the structure and frequency calculations, we also analyzed the spin populations and charges on the atoms in the QM region resulting from the optimizations. Spin populations and Mulliken charges were determined in the usual way.[52] As Mulliken charges are known to give unreliable values in many cases, charges derived by a fitting of the electrostatic potential (ESP) were also determined. We used the following three-step procedure:[56]

(1) A set of points was chosen randomly around the active site with the constraint that the points should be placed no closer to any atom than its Born radius and no further away than 5 Å.[57] We found that 4000 points per structure was appropriate for our calculations.

(2) The electrostatic potential was calculated at each point using the same DFT approximation and electron density as in the hybrid potential calculations.

(3) The charges on the atoms in the QM region were fit to the electrostatic potentials using a standard linear least-squares algorithm. In the fitting procedure the sum of the fitted charges was constrained to be equal to the actual total charge of the structure in the hybrid potential model.

3. Results and Discussion

3.1. Influence of the Protein Matrix on the Active Center. There has been some debate as to whether it is really necessary to include the protein when modeling the hydrogenase active site. In our view, we think it reasonable to suppose that the protein matrix will have an influence on the active site of hydrogenase which is deeply buried inside the protein. This influence could manifest itself in a number of ways. Some examples are as follows:

(a) It is evident by analyzing the crystal structure that there will be severe steric constraints that make certain configurations of the atoms in the active site unlikely. Thus, for example, steric effects strongly suggest that the three ligands of the Fe atom are non-exchangeable.[16] They would also seem to preclude the model proposed by Pavlov et al. in which a cyanide ligand leaves its pocket to become a bridging ligand of the bimetallic center (lack of experimental evidence, see Figure 1b).

(b) Another important feature constraining the cyanide ligands is their hydrogen bonds to the protein (see Figure 1a).

(c) There is a single entrance to the active site that points to the nickel in the vicinity of Cys 530.[47,48] Entering species, such as H_2, are likely to encounter the Ni atom before the Fe atom. In some Ni−Fe hydrogenases Cys 530 is replaced by a selenocysteine indicating its unique character compared to the other three cysteines at the active site. This residue and its protonation state seem to play a crucial role in the enzymatic reaction,[20] and so it is important to include it entirely in the simulation.

(49) Van Der Zwaan, J. W.; Coremans, J. M. C. C.; Bouwens, E. C. M.; Albracht, S. P. J. *Biochim. Biophys. Acta* **1990**, *1041*, 101−10.

(50) Churchill, M. R.; Bueno, C.; Park, J. T.; Shapley, J. R. *Inorg. Chem.* **1984**, *23*, 1017−21.

(51) Fan, C.; Teixeira, M.; Moura, J.; Moura, I.; Huynh, B. H.; Le Gall, J.; Peck, H. D. J.; Hoffman, B. M. *J. Am. Chem. Soc.* **1991**, *113*, 20−24.

(52) The Cambridge Analytic Derivatives Package Issue 6, Cambridge 1995. A suite of quantum chemistry programs developed by R. D. Amos with contributions from I. L. Alberts, J. S. Andrews, S. M. Colwell, N. C. Handy, D. Jayatilaka, P. J. Knowles, R. Kobayashi, K. E. Laidig, G. Laming, A. M. Lee, P. E. Maslen, C. W. Murray, J. E. Rice, E. D. Simandiras, A. J. Stone, M.-D. Su, and D. J. Tozer.

(53) Dunning, T. H., Jr.; Hay, P. J. *Modern Theoretical Chemistry: Methods of Electronic Structure Theory*; Schaefer, H. F., III, Ed.; Plenum: New York, 1977; Vol. 3.

(54) Hay, P. J.; Wadt, W. R. *J. Chem. Phys.* **1985**, *82*, 270−83, 299−310.

(55) Glukhovtsev, M. N.; Bach, R. D.; Nagel, C. J. *J. Phys. Chem. A* **1997**, *101*, 316−23.

(56) Hinsen, K.; Roux, B. *J. Comp. Chem.* **1997**, *18*, 368−80.

(57) Mouesca, J. M.; Chen, J. L.; Noodleman, L.; Bashford, D.; Case, D. A. *J. Am. Chem. Soc.* **1994**, *116*, 11898−914.

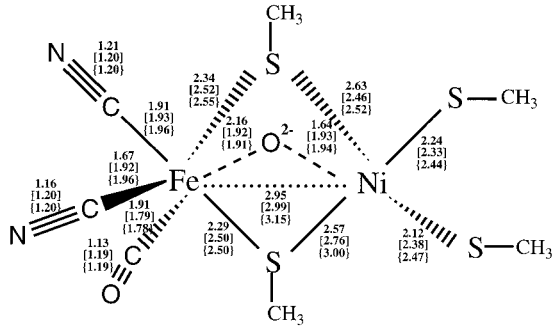

Figure 6. Comparison of the distances in the active site of the Ni−A form: (1) the X-ray data (no brackets), (2) active site simulated in the protein matrix (square brackets), and (3) active site simulated in vacuum (curly brackets).

Table 1. Percentage Bond-Stretching Character of the Three Frequencies Identified as Belonging to the 3 Nonproteic Ligands Bound to the Fe Atom of the Active Site

environment	ν_{sim} (cm^{-1})	% CO	% CN_1^-	% CN_2^-
in the protein	1907	96.7	0.2	0.2
matrix	2083	0.1	91.5	7.4
	2097	0.3	7.4	91.4
in vacuum[b]	1874	96.7	0.1	0.2
	2076	0.4	61.0	37.7
	2081	0.0	37.8	61.2

[a] Values are given for a model of the Ni−A structure in vacuum and in the protein matrix ($S = {}^3/_2$). [b] Methyl blocked cysteines (all minimized).

(d) The electrostatic field produced by the amino acid residues surrounding the active site could have considerable influence on the energetics of any reaction process taking place at the active site. This effect would seem to be difficult to reproduce in vacuum calculations.

Calculations of the Ni−A form of the active site, in vacuum and in the protein matrix, were performed to test the importance of including the protein. For the vacuum test, we used the same number of QM atoms as in the hybrid potential model of Ni−A but left out all the MM atoms. Figure 6 shows the optimized structures we obtained for the Ni−A form (spin state $S = {}^3/_2$) in vacuum. The X-ray distances of the 2.54 Å resolution model for the oxidized form are also shown. Vacuum-based distances around the Ni atom are longer than those observed in the X-ray crystallographic structure and in the structure optimized using the hybrid potential. We have observed the same trend for vacuum calculations of the Ni−SI2 and the Ni−R forms. In addition, the Fe−C−N and the Fe−C−O angles are linear for the in vacuum structures whereas this is not so for the structures which included the protein.

We have also determined frequencies for the three nonproteic ligands for the optimized structure in vacuum as well as the structure in the protein. These values are shown in Table 1 along with the percentage bond stretching character for each ligand. It is clear that the in vacuum frequencies are very different, being lower, than those resulting from the DFT/MM calculations. The values of the percentage stretching for each frequency indicate that the calculations in vacuum introduce an artificial symmetry for the cyanide ligands that does not exist in the protein. With the hybrid potential, the three frequencies correspond strictly to the stretching of one particular bond.

In summary, we concluded that the protein has a significant influence on the active site and so all our subsequent work was done including it.

3.2. Spin and Charge Analysis. Investigating the spin state of the active center of hydrogenase is a delicate matter owing to the complexity of the system. Here we summarize our attempts in our simulations to match the spin states to the EPR data. The atomic spin populations of several spin states $\{S, S^2 \equiv S(S+1)\}$ for the different redox forms are given in Table 2.[58] The common feature of all states is that there is no significant spin population on the Fe, a result that is in agreement with a recent ENDOR study.[14] This can be explained by the presence of the two CN^- and the CO molecules which are strong ligands and maintain the iron in a low spin and low oxidation state, most probably Fe(II), in all cases.[13] There is also no major change in the spin of the sulfur atoms, and this suggests that there is no sulfur radical formation.[29]

The oxidized form Ni−A is EPR active with a total spin, S, of ${}^1/_2$. As shown in Table 2, we considered spins of ${}^1/_2$ and ${}^3/_2$ in our study. We encountered some spin contamination problems for the $S = {}^1/_2$ case and the final structure has a S^2 value of 1.37. Test calculations on the molecule $[Ni^{III}-O^{-II}]^+$, however, show that both the value of S^2 and the way in which the spin is partitioned are very sensitive to the Ni−O distance. In contrast, the $S = {}^3/_2$ case is not contaminated. The atomic spin population on the Ni atom is perhaps smaller than could be expected (it should be around 3 for Ni(III)) with the remainder of the spin spread onto the bridging oxo group and, to a lesser extent, on the sulfur atoms. The $S = {}^3/_2$ form is not observed experimentally. For the $S = {}^1/_2$ state, the spin of ${}^1/_2$ on the nickel atom (spin population around 1) could imply Ni(I) as well as Ni(III), yet it is more likely that in this oxidized form of the enzyme, the formal charge of Ni is III.[14]

The spin states of Ni−SI2 and Ni−R are, in principle, easy to deal with as both forms are EPR silent. However, owing to some problems with convergence of the DFT calculations at the beginning of the study we looked, in the end, at the $S = O$ and 1 states for both forms. The zero spin on each atom of the active center implies a Fe(II)−Ni(II) center bound to a hydride (for both the Ni−SI2 and the Ni−R $S = O$ states). For reasons which will become clear in the next section it seems unlikely that model 1 of Ni−R (see Figure 5) is correct as the proton placed on Cys 65 migrated away from the S-atom with a significant hydride ion character. As Ni−C has a total spin of ${}^1/_2$, two different structures with $S = {}^1/_2$ were studied and were discriminated between using the results of the IR analysis (see below). The atomic spin populations for both models are quite similar; most of the spin is located on the Ni and corresponds to Ni ($S = {}^1/_2$), i.e., Ni(I) or Ni(III).

ESP and Mulliken charges for most atoms of the active site are given in Table 3. The most obvious point is the difference in the values of the ESP and Mulliken charges. This is well established and consequently care must be taken when analyzing the charges in order not to assign too much weight to their absolute values. There are, however, a number of trends that can be noted. The hydrogen species bridging the bimetallic center are always hydrides. Thus, for the Ni−SI2 state, given the spin analysis and the charge of the bridging ligand, the arrangement $Fe^{II}-H^-Ni^{II}$ is favored over $Fe^{I}-H^+-Ni^{I}$. This result supports recent EPR studies.[28] The charge analysis shows that bridging thiolates are, in general, less negatively charged than the terminal ones (due to a stronger interaction with the metals), and that, between the different redox states, the major changes in the sulfur charges occur when a cysteine goes from an unprotonated to a protonated form. Finally, we note that, in contrast to the ESP charges, the shifts of the Mulliken charges

(58) If the total spin S is located on one atom then the spin population of that atom should be twice the value of S (typically around 70% of that value).

Table 2. Atomic Spin Analysis for Each Redox State of the Hydrogenase[a]

			spin analysis								
	S	S^2	Fe	Ni	S_{65}	H^+_{65}	S_{68}	S_{530}	H^+_{530}	S_{533}	L_{bridge}[c]
A	1/2	1.37	−0.12	1.17	0.04	N/A	0.07	0.07	N/A	0.19	−0.48
	3/2	3.76	0.06	1.35	0.09	N/A	0.22	0.27	N/A	0.17	0.86
SI2	0	0	0	0	0	0	0	0	0	0	0
	1	2.01	0.05	1.31	0.11	N/A	0.09	0.22	N/A	0.19	0.02
$C(H^+_{530})$	1/2	0.77	0.03	0.90	0.03	N/A	0.03	0.02	0.00	0.00	0.01
$C(H^+_{65})$	1/2	9.87	0.01	1.05	−0.05	−0.16	0.02	0.05	N/A	0.09	0.01
R(1)	1	2.01	−0.02	1.11	0.22	0.54[d]	0.06	0.01	0.01	0.05	0.00
R(2)	0	0	0	0	0	0	0	0	0	0	0

[a] Notes: (1) The lowest value for the total spin corresponds to the experimental value; (2) the spin populations of the 3 nonproteic ligands were all very close to zero and so are not given in the table. [c] Ligand bridging the bimetallic center: O^{2-} (Ni−A), H^- (Ni−SI2, Ni−C, Ni−R). [d] In the simulation, this proton did not stay on the sulfur.

Table 3. ESP and Mulliken Charges (the First and Second Numbers, Respectively) of the Main Atoms of the Active Site (No Significant Changes Were Found for the Charges of the CN^- and CO Ligands)

		charge								
	S	Fe	Ni	S_{65}	H^+_{65}	S_{68}	S_{530}	H^+_{530}	S_{533}	L_{bridge}[a]
A	1/2	0.46, 0.00	1.02, 0.29	−0.88, −0.44	N/A	−0.51, −0.20	N/A	−0.09, −0.14	−0.90, −0.14	−0.90, −0.66
	3/2	0.15, 0.01	0.81, 0.32	−0.78, −0.44	N/A	−0.39, −0.17	−0.49, −0.18	N/A	−0.31, −0.18	−0.70, −0.61
SI2	0	0.72, −0.20	0.68, 0.01	−0.79, −0.41	N/A	−0.42, −0.14	−0.57, −0.15	N/A	−0.40, −0.18	−0.57, −0.12
	1	0.26, −0.22	0.98, 0.10	−0.90, −0.44	N/A	−0.42, −0.19	−0.46, −0.18	N/A	−0.29, −0.13	−0.58, −0.13
C(530)	1/2	0.50, −0.24	0.52, 0.02	−0.86, −0.53	N/A	−0.41, −0.21	−0.29, 0.06	0.20, 0.13	−0.32, −0.19	−0.65, −0.17
C(65)	1/2	0.43, −0.23	0.41, 0.00	−0.16, 0.06	−0.28, −0.27	−0.57, −0.22	−0.62, −0.22	N/A	−0.37, −0.19	−0.49, −0.17
R(1)	1	0.43, −0.24	0.51, −0.01	−0.44, −0.25	−0.45, −0.38[b]	−0.60, −0.21	−0.40, 0.06	0.20, 0.13	−0.31, −0.17	−0.43, −0.11
R(2)	0	0.51, −0.20	0.87, −0.26	−0.97, −0.43	−0.41, −0.08[c]	−0.60, −0.22	−0.11, 0.04	0.12, 0.09	−0.28, −0.15	−0.55, −0.10

[a] Ligand briding the bimetallic center: O^{2-} (Ni−A), H^- (Ni−SI2, Ni−C, Ni−R). [b] In the simulation, this proton did not stay on the sulfur and took a hydride character. [c] This is the charge of the hydride placed on the axial binding site of the Ni.

for the Ni agree very well with the XAS results on the Ni absorption edge.[30]

3.3. Structural Results. Some interatomic distances determined using the optimized structures of the different redox intermediates for the hydrogenase active site are presented in Table 4. The most striking structural change between the states is the shortening of the Ni−Fe distance on going from the most oxidized to the most reduced form. This difference is in agreement with crystallographic[20] and EXAFS experiments.[30] Part of this change, although by no means all, is due to the steric effect of the bridging ligand—an oxo group will keep the metals further apart than a hydride.

The distances in Table 4, calculated for the Ni−A form, are similar to those for the X-ray "as-prepared" oxidized structure. Both spin states ($S = {}^1/_2$ and ${}^3/_2$) are broadly similar although there are two principal differences:

(1) The Ni−Fe distance is 2.89 Å in the $S = {}^1/_2$ form and 2.99 Å in the $S = {}^3/_2$ form. Both these values are within the range of those observed for the X-ray structures of the oxidized form of the hydrogenases from *D. gigas*, 2.94 Å,[13] and from *D. fructosovorans*, 2.90 Å.[19]

(2) The bridging oxo group is equidistant from both metals in the $S = {}^3/_2$ form while it is slightly asymmetric (closer to the Ni) in the $S = {}^1/_2$ form. A stronger asymmetry was observed in the X-ray structure of *D. gigas* hydrogenase and the higher resolution structure of *D. fructosovorans* hydrogenase. The angle Fe−O−Ni of 100° also compares well with the experimental data.

The structures of the Ni−SI2 forms ($S = 0$ and 1) have identical Ni−Fe distances which are intermediate between those of the Ni−A and Ni−R forms. The major differences lie in the bond length of Ni to the sulfur of Cys 533 and in the position of the bridging hydride which is closer to the Ni atom in the $S = 0$ state. We also optimized a structure for a model of Ni−SI1 ($S = 0$) (the model we used for Ni−SI1 is Fe^I−Ni^I with no exogenous bridging ligand). This, however, results in a structure with a very long Ni−Fe distance of 3.23 Å and longer bond distances in the rest of the structure as well, compared to the other redox forms.

Table 4. Active Site Bond Distances for the Optimized Structures of the Ni−A, Ni−SI2, Ni−C, and Ni−R forms of hydrogenase[a]

	d (Å)					
	X−ray	Ni−A: 1/2, 3/2	Ni−SI2: 0,1	Ni−C: H^+_{530}, H^+_{65}	Ni−R:[c] 1	Ni−R:[d] 0
Ni−S65	2.12	2.32, 2.38	2.27, 2.41	2.45, 2.55	2.34	2.35
Ni−S68	2.57	2.69, 2.76	2.36, 2.61	2.52, 2.56	2.52	2.76
Ni−S530	2.24	2.33, 2.33	2.31, 2.37	2.53, 2.32	2.74	2.78
Ni−S533	2.63	2.50, 2.46	2.82, 2.44	2.64, 2.41	2.47	2.50
Ni−Fe	2.95	2.89, 2.99	2.74, 2.74	2.77, 2.73	2.633	2.68
Ni−L_{bridge}[b]	1.64	1.86, 1.93	1.64, 1.79	1.82, 1.93	1.78	1.61
Fe−L_{bridge}	2.16	1.91, 1.92	1.79, 1.69	1.70, 1.69	1.68	1.77
Fe−S68	2.29	2.56, 2.50	2.44, 2.46	2.49, 2.51	2.49	2.51
Fe−S533	2.22	2.46, 2.52	2.40, 2.46	2.42, 2.49	2.53	2.39

[a] Fe−C (CN^-) distances are within 1.92 and 1.96 Å while Fe−C (CO) are within 1.78 and 1.90 Å. The C−N and C−O distances are 1.20 and 1.18 Å, respectively. [b] Ligand bridging the bimetallic center: O^{2-} (Ni−A), H^- (Ni−SI2, Ni−C, Ni−R). [c] This form had originally a H^+ on Cys 65 which takes a hydride character (S_{65}-H^- = 2.31 Å). [d] This form has a hydride in the vacant axial coordination site of the nickel (Ni−H^- = 1.52 Å).

We investigated two possibilities for the Ni−C state (either protonated Cys 530 or Cys 65) and both give reasonable structures. One indication in favor of the second model (Cys 65 protonated) is the larger Ni−H^- distance of 1.93 Å (as opposed to 1.82 Å) which could explain the low hyperfine coupling observed in the Ni−C EPR signal.[51] To really discriminate between the structures, however, the IR data described in the next section are needed.

Model 1 of Ni−R seems to be chemically unlikely as the proton that we had placed on Cys 65 moves away and ends up at 2.31 Å from the sulfur with a negative charge (see Table 3). Model 2 with a hydride in the second vacant binding site of

Table 5. Infrared Frequencies Corresponding to the 3 Nonproteic Ligands (2 CN^- and 1 CO), of the Fe Atom in the Active Site

redox states	form	IR freq: normal mode anal.: CO, $CN^-_{1,2}$: $\nu_{cm^{-1}}$
Ni−A	exp	1947, 2083, 2093
	$S = 1/2$	1896, 2081, 2091
	$S = 3/2$	1907, 2083, 2097
Ni−SI2	exp	1934, 2075, 2086
	$S = 0$	1886, 2058, 2073
	$S = 1$	1900, 2076, 2086
Ni−C	exp	1952, 2073, 2086
(H^+_{530})	$S = 1/2$	1884, 2051, 2079
(H^+_{65})	$S = 1/2$	1903, 2065, 2081
Ni-R	exp	1940, 2060, 2073
(1)	$S = 1$	1884, 2059, 2072
(2)	$S = 0$	1895, 2061, 2078

the Ni atom appears to be more favorable as will become apparent when we consider the results of the normal mode calculations.

In all the optimized structures, the hydrogen bonds to the cyanide ligands of the Fe atom that are observed in the X-ray structure are preserved. Due to the van der Waals interactions with the protein environment, the Fe−C−N and Fe−C−O angles are never at 180° but always slightly bent.

3.4. Normal Mode Analysis. The IR frequencies of the CN^- and CO ligands are shown in Table 5. It is apparent that the frequencies corresponding to the CN^- bond stretching modes are in excellent agreement with experimental data. Both the shifts between the different redox states and the absolute values of the frequencies are well reproduced. The results for CO are not as good. Whereas the directions of the shifts in the frequencies between states are correct, their magnitudes are too small. In addition, the absolute values of the CO frequencies are systematically underestimated. This underestimation is probably a result of the DFT method that we have used (free CO: calculated 2027 cm^{-1} versus 2143 cm^{-1} experimentally) but it could also be due to inaccuracies arising from the QM/MM interaction part of the hybrid potential for the CO molecule. In contrast, the CN^- environment is well modeled as the hydrogen bonds with the protein matrix are conserved in all our calculations.

The frequencies for our model of Ni−A for both the $S = {}^1/_2$ and ${}^3/_2$ states are in good agreement with experiment although the $S = {}^1/_2$ state wavefunction has a high degree of spin contamination.

Given the structural results we obtained for the Ni−SI1 ($S = 0$) state, we expected that the frequencies would not compare well with experimental data. Indeed, we found $\upsilon = 1734$, 2010, 2024 cm^{-1} which are far from the experimental values of $\upsilon =$ 1914, 2055, 2069 cm^{-1}. These results are not in the table.

For the Ni−SI2 state, we studied the $S = 0$ and 1 spin states. Whereas the $S = 1$ results are comparable to the experimental values for the Ni−SI2 state, the $S = 0$ results are in surprisingly good agreement with the Ni−SI1 experimental values. This result, together with the poor results we obtained for our model of the Ni−SI1 state, casts doubt on the hypothesis of a Ni−SI1 form consisting of a Fe^I−Ni^I cluster with no bridging ligand surrounded by deprotonated cysteines. It implies that a bridging hydride could also be present in the Ni−SI1 form and that an additional proton on Ni−SI2 is located elsewhere. The presence of a hydrogen species tightly bound to the Ni atom in both SI forms could explain the high activation energy observed for their anaerobic oxidation to form B.[16]

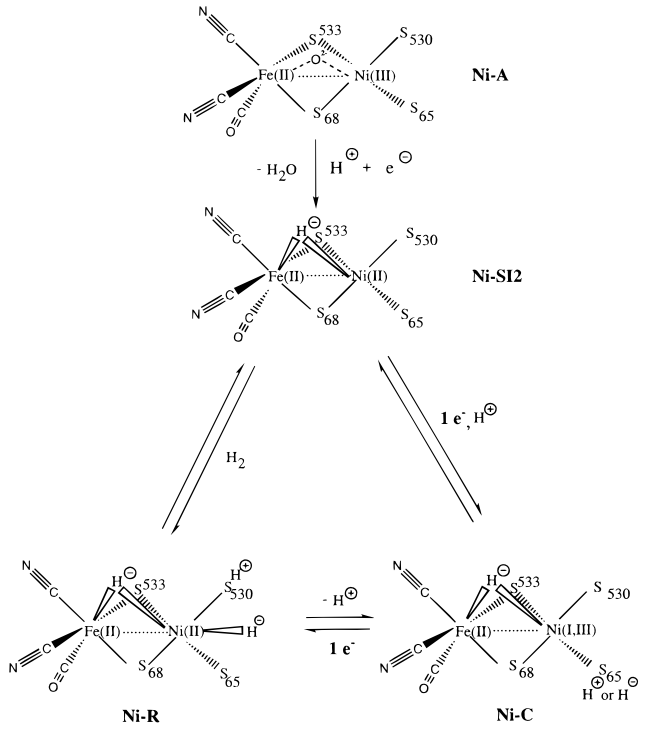

Figure 7. The most probable mechanism suggested by our simulations.

For the remaining forms, Ni−C with Cys 65 protonated and the second model of Ni−R, in which a hydride binds to the remaining Ni coordination site, appear to us the most probable and give frequency shifts that are in the best agreement with experiment.

3.5. Catalysis. The results of our calculations lead us to suggest the catalytic cycle that is shown in Figure 7. Ni−A consists of a Fe^{II}−Ni^{III} bimetallic center asymmetrically bridged by an oxo group. This form, although it is not part of the catalytic cycle, is important as it is the form that was first obtained by crystallography and it is believed to participate in the activation/inactivation process of the enzyme.[16] Upon reduction of the enzyme, the loss of the oxo bridge leaves an empty binding site for the hydrogen species which are produced from the H_2 redox chemistry at the active site. The Ni−SI2 form is well modeled as a Fe^{II}−Ni^{II} center with a bridging hydride. We have not been so successful with the Ni−SI1 form and we think that part of the problem resides in whether there is a ligand bridging the bimetallic center or not. The product of the heterolytic cleavage of H_2, namely H^+ and H^-, binding to Ni−SI2 gives the Ni−R form by protonation of Cys 530 and binding of a hydride to the vacant axial coordination site of the nickel (model 2 of Ni−R). Thus, as expected, the thiolate of Cys 530 acts as a base that assists the Ni in binding molecular hydrogen. The EPR active Ni−C form is obtained from Ni−SI2 by reduction of Ni(II) to Ni(I) together with protonation of Cys 65. We note that for the Ni−C form, the charge of the proton placed on Cys 65 is actually negative on the optimized structure. This suggests the electron density is delocalized on the proton of Cys 65 which would be in agreement with XAS experiments that do not see significant electron density changes at the Ni atom.[30] Going from Ni−R to Ni−C, one electron presumably goes to the proximal 4Fe−4S cluster, the axial hydride moves to Cys 65, and the first proton to leave the active site is located at Cys 530, close to the substrate entrance to the active site[48] and to Glu 18, a plausible component of a proton transfer channel (unpublished).

4. Conclusion

In this work, we have studied several redox intermediates of hydrogenase that are believed to be involved in the catalysis of molecular hydrogen to obtain insights into the enzymatic reaction. The hybrid DFT/MM potential that we used appears to model remarkably well this complex metalloenzyme as the results of our simulations are, by and large, in good agreement with the available experimental X-ray, EPR, and IR data. The assumption that we made in devising the catalytic cycle of minimal conformational changes for the active enzyme with respect to the X-ray structure of the oxidized inactive form has been recently confirmed by the crystal structure of a reduced form of the NiFeSe hydrogenase from *Desulfomicrobium baculatum*.[20]

Our results lead us to the following remarks: (1) The "special" role of Cys 530, located at the H_2 entrance of the active site, is confirmed in our calculations as its protonation (which is not equivalent to the protonation of Cys 65) seems to play the role of a base in the mechanism. (2) Our calculations imply that the Fe atom is not redox active. Rather, it stays in a low-spin Fe(II) state stabilized by the 3 nonproteic ligands. (3) The Ni atom (formal redox states from I to III, and I to II in the catalytic cycle), the terminal S-ligands, and the hydrogen species are the atoms involved in redox chemistry. (4) Our results do not favor an involvement of sulfur radicals. (5) Ni−SI1 might contain a bridging hydride and thus there might be an extra proton in the active site for all the redox forms in the catalytic cycle.

Finally, we would like to emphasize that, owing to the expense of these calculations, we did not perform an exhaustive investigation of all possible binding sites and spin states for each redox form. However, the quantitative agreement that we have obtained with the experimental data shows that we have a reasonable picture of some of the structures that constitute the catalytic cycle of hydrogenase.

There are a number of extensions to this work that can be envisioned. These include a study of the dynamics of H_2 binding to the active site and an investigation of the redox states of the Fe−S clusters. From an experimental point of view, high-resolution X-ray data for the different redox states of the enzyme, which would provide a more detailed picture of the structure of the active site at various points along the catalytic cycle, could help further theoretical calculations.

Acknowledgment. The authors would like to thank Drs. M. Frey, K. Hinsen, J.-M. Mouesca, and A. Thomas for helpful discussions and the Commissariat à l'Energie Atomique and the Centre National de la Recherche Scientifique for support of this work. This work was partially supported by Grant CT-94-2041 from the European Union Biotechnology program.

JA983971B